UV-activated paramagnetic centers in high-κ zirconia-silica thin films

Robert N. Schwartz,[1,2] Heinrich G. Muller,[1,*] Peter D. Fuqua,[1] James D. Barrie,[1] and Robert B. Pan[1]
[1]*The Aerospace Corporation, El Segundo, California 90245, USA*
[2]*Department of Chemistry and Biochemistry, University of California–Los Angeles, Los Angeles, California 90024, USA*
(Received 16 June 2009; revised manuscript received 6 August 2009; published 1 October 2009)

Amorphous thin films of $Zr_xSi_{(1-x)}O_2$ have been prepared on fused silica substrates and investigated by electron paramagnetic resonance spectroscopy. A defect center was identified at $g=2.0085\pm0.0004$ that is UV-light activated and photoquenched by red visible light. Its appearance is shown to depend on the amount of silicon in the films. Based on experimental results presented here as well as studies in other oxide-based materials such as amorphous SiO_2, we suggest that the UV-induced center in amorphous ZrO_2(Si) films is an *oxygenic-hole* center.

DOI: 10.1103/PhysRevB.80.134102 PACS number(s): 76.30.Mi, 73.50.Gr

I. INTRODUCTION

The formation of point defects/color centers can lead to significant degradation to material function. An in-depth understanding of point defects, at the atomic level, is crucial for evaluating the performance of a material in specific electrical and optical devices, as well as for developing material fabrication techniques to eliminate them.

In recent years, zirconia has become one of the most investigated materials. Among its numerous applications is its use as an oxygen conductor,[1] high-κ dielectric on silicon circuits,[2–4] and for fabricating antireflective dielectric coatings for solar panels used in spacecraft applications.[5] As an alternative gate dielectric for silicon-based microelectronic devices, alloys of ZrO_2 with SiO_2 show great promise and currently, significant research is devoted to assessing material stability and to developing a microscopic understanding of potential defect structures distributed throughout the thickness of the film and at the interface between the silicon substrate and the dielectric layer.[4,6–8]

In this paper, we use electron paramagnetic resonance (EPR) to investigate the formation of defect centers in amorphous zirconia-silica mixtures (a-$Zr_xSi_{(1-x)}O_2$). In particular, the work reported here focuses on a paramagnetic center(s) that is activated by irradiation with UV light at 253.7 nm and photoquenched by irradiation with red light at 623 nm.

II. EXPERIMENTAL DETAILS

All films were deposited on fused silica substrates (Corning 7980) purchased from United Lens Co., Inc. Thin films of zirconia, mixed with various amounts of silica and designated as ZrO_2(Si), were rf-sputtered from the elements in a low-pressure oxygen atmosphere. Silica contents ranged from nominally zero to as much as 99%. In addition, *multilayer stacks* consisting of alternating layers of zirconia (also doped with various amounts of silica) and pure silica were fabricated. These structures have a large number of zirconia-silica interfaces and provide an opportunity to assess if these interfaces contribute substantially to the occurrence of any specific defects. The percentage of silica in ZrO_2(Si) was determined with *secondary-ion mass* spectroscopy by sputtering off the surface some 20–50 nm in thickness and using the equilibrium ion yields that would arise after the typical surface peaks had been sputtered away. For one film, the result was subsequently confirmed to within 1% by energy dispersive x-ray analysis.

X-ray diffraction measurements (not reported here) revealed that all films were amorphous, with the exception of the nominally pure ZrO_2 film which exhibited the peaks of monoclinic zirconia. Annealing experiments were carried out in a Lindberg single-zone tube furnace. Single-layer films were annealed in either forming gas (FG) (5% H_2, 95% N_2) or air for 10 h at 350 °C. The multilayer stacks were annealed for 2.5 h at 460 °C in the same gases. It should be noted that all anneals were intentionally carried out well below 900 °C in order to prevent phase separation into a heterogeneous mixture of nanocrystallites of ZrO_2 and SiO_2.

All EPR measurements were carried out at 77 K using an X-band homodyne Varian E-Line Century Series spectrometer utilizing a TE_{102} rectangular microwave cavity with 25 kHz magnetic-field modulation. The spectrometer is equipped with a Bruker B-H15 magnetic-field controller; the applied magnetic-field values were calibrated by means of a proton magnetic-resonance Gaussmeter. The microwave frequencies were measured using a Hewlett-Packard 5342A automatic frequency counter. To achieve a reasonable signal-to-noise ratio, all spectra reported here were signal averaged over five scans. The sample disks (substrate plus film) were cut into 16 mm(l)$\times$3 mm(w)$\times$1.6 mm(h) rectangular parallelepipeds (with thin-film volume $\sim 7-8\times10^{-5}$ cm^3). Given these dimensions, two samples fit into the portion of a standard EPR liquid nitrogen insertion dewar that extended through the microwave cavity. First, EPR spectra of the samples were taken prior to UV exposure. Then, the samples were transferred from the EPR insertion dewar, without warming, to another liquid nitrogen-cooled dewar and exposed to UV radiation. This procedure was necessary to avoid color center formation in the fused silica components of the EPR dewar. UV light was provided from a Penn-Ray mercury vapor lamp with more than 96% of emitted light at 253.7 nm. After UV illumination for 15 min, the samples were transferred back to the EPR dewar system. Then, after recording the EPR spectra of the UV-irradiated film, red light from a dye laser (623 nm) was introduced to the cavity through a multimode fiber to expose the samples *in situ* to "bleaching (photoquenching)" light ($\sim$150 mW). The

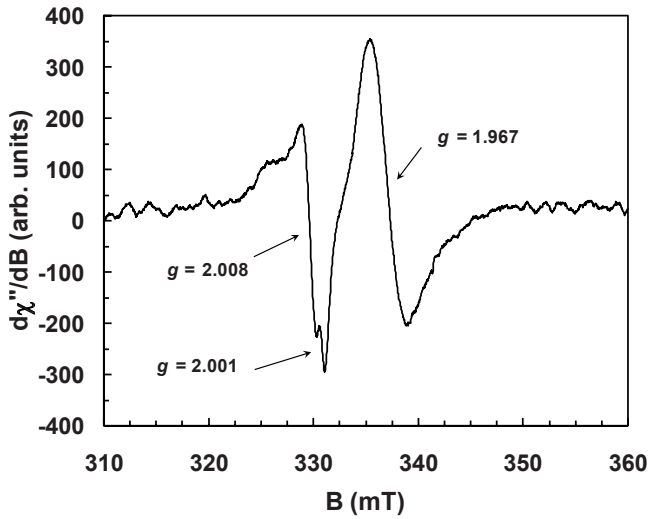

FIG. 1. EPR spectrum at 77 K of as-deposited ZrO_2(Si) film before exposure to UV. The spectrometer settings are gain=320 and ν=9.263 48 GHz.

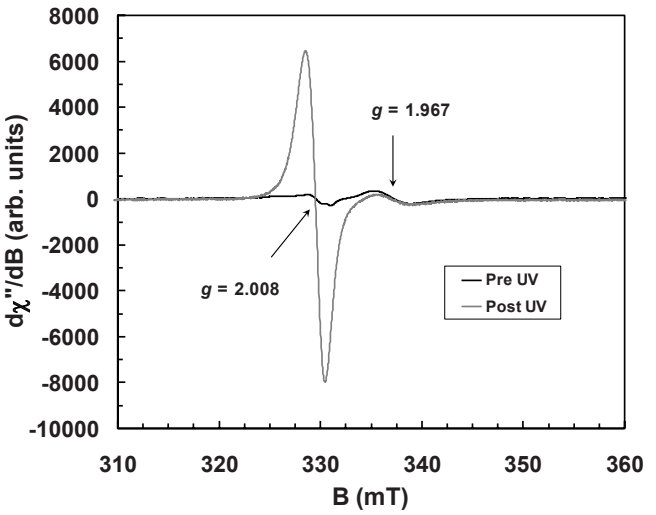

FIG. 2. EPR spectrum at 77 K of as-deposited ZrO_2(Si) film after exposure to UV. The spectrometer settings are gain=320 and ν=9.263 48 GHz. Also included in the figure is the pre-UV spectrum shown in Fig. 1.

changes induced were subsequently revealed by recording EPR with the 623 nm light off. Variable temperature EPR measurements were carried out with a Bruker EMX *X*-band spectrometer equipped with a Bruker variable-temperature control unit. A Bruker dual-cavity configuration, in conjunction with a known spin standard, was used to determine the concentration of paramagnetic centers in the films.

III. RESULTS

All the EPR data reported in this section were obtained on films containing ~15% SiO_2. The results for films fabricated with varying amounts of SiO_2 will be presented below in Sec. IV A. The reported EPR absorption spectra, recorded as $d\chi''/dB$, are expressed in terms of arbitrary units. Absolute concentration measurements of the paramagnetic UV-induced centers were made in a limited number of samples. Therefore, care must be exercised when comparing the spectral intensities of the spectra presented in the figures below, since even relative comparisons using derivative spectra can be tricky and require careful consideration of such factors as instrumental settings, spectral line shapes, sample sizes, etc.[9] These factors were taken into account when analyzing the spectra and are reflected in the interpretation of the data. The estimated uncertainty for the reported *g*-factor values, measured at zero crossing, is in the range of $\pm 0.001 - \pm 0.0004$ depending on the line shape of the resonance. For all spectra reported below, the following spectrometer settings were used: microwave power=1 mW and modulation amplitude =3.2 G.

A. As-deposited ZrO_2(Si) films

Shown in Fig. 1 is the EPR spectrum recorded at 77 K of an as-deposited Si-doped ZrO_2 film [single layer ~1.5–1.6 μm thick, ~15% Si, and designated as ZrO_2(Si)] *before* being subjected to UV illumination. Several spectral features with *g*-factor values of 1.967, 2.008, and 2.001 are clearly visible and their significance will be discussed below. Figure 2 compares the EPR spectra recorded at 77 K before and after UV exposure (at 77 K). The intensity of the spectra, which have been corrected for the spectrometer gain, clearly reveals that UV irradiation generates a strong spectral feature at g=2.008. It should also be noted here, as well as in other figures to be presented, that the g=1.967 spectral feature remains unchanged.

We also recorded the EPR of the fused-silica substrate before and after UV irradiation. Prior to UV irradiation, no EPR signal was observed at 77 K. However, after UV irradiation at 77 K, an EPR resonance (g=2.002, also recorded at 77 K) was observed which is quite small relative to the EPR signals from the ZrO_2(Si) films UV irradiated under the same conditions. In addition, the UV-induced substrate signal is not photoquenched by the 623 nm light. This is important since the *difference* spectra described below are free from interference from EPR signals assigned to the substrate.

Figure 3 presents EPR spectra recorded following UV irradiation and then exposed for various lengths of time to 623 nm light. It should be emphasized that all EPR measurements as well as exposure to UV and 623 nm light were

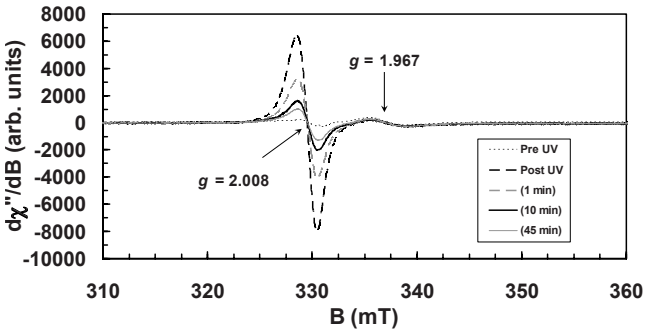

FIG. 3. EPR spectra of as-deposited ZrO_2(Si) film measured at 77 K. Sample first irradiated with UV then followed by illumination with 623 nm light for 1, 10, and 45 min (gain=320).

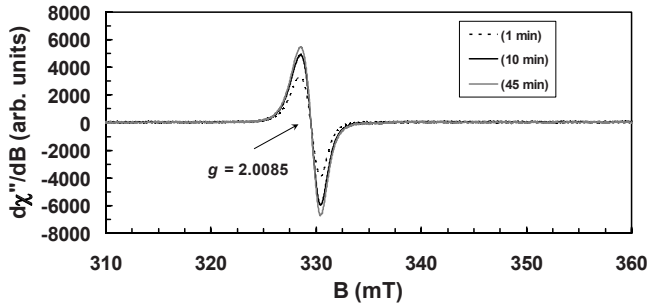

FIG. 4. EPR difference spectra of as-deposited ZrO_2(Si) film measured at 77 K. Sample first irradiated with UV then followed by illumination with 623 nm light for 1, 10, and 45 min (gain=320). The spectra measured after 623 nm illumination were subtracted from the post-UV EPR spectrum.

carried out at 77 K; the sample never warmed above 77 K over the duration of the data collection. It is clear from these spectra that exposure to 623 nm leads to a reduction in the UV-induced EPR signal at $g=2.008$, whereas the signal at $g=1.967$ remains unchanged.

In this paper, only data related to the photoquenching effects of 623 nm light are presented; however, a limited number of measurements were made using light of different wavelengths. It was observed that exposure to 514 nm light led to the reduction in the UV-induced EPR center, whereas exposure to longer wavelength light, such as 980 nm light, had no effect on the EPR of the UV-induced center.

In Fig. 4, EPR *difference* spectra are displayed to illustrate the color center photoannealing with 623 nm light. As indicated in the inset, these spectra are obtained by subtracting from the *post* UV spectrum the EPR spectra following photoquenching with 623 nm light for the various exposure times. Clearly visible is a single EPR feature at $g=2.0085\pm0.0004$ and peak-to-peak linewidth $\Delta B_{p\text{-}to\text{-}p} \approx 19$ G, which is induced by exposing the ZrO_2(Si) film to UV irradiation and photoquenched when subjected to 623 nm light. From comparison to known spin standard, we estimate that the concentration of paramagnetic UV-induced centers with $g=2.0085$ is in the range of $1-3\times10^{18}$ centers/cm^3 for the as-deposited films.

B. Annealed ZrO_2(Si) films

Samples cut from the same disk, which were used in the study reported in the above section, were annealed in a tube furnace for 10 h at 350 °C in air or forming gas. The EPR spectra of the annealed samples prior to UV irradiation are shown in Fig. 5. The air-annealed sample displays only a single EPR feature at $g=1.967$, whereas the forming-gas-annealed sample exhibits a feature at $g=1.967$ and an additional resonance at $g=2.0015$. These samples were then UV irradiated; the results for both annealed samples were similar. For brevity, we only show the difference EPR spectra for the air-annealed sample in Fig. 6. Similar to the as-deposited films, the additional EPR feature at $g=2.0085$, which is induced by exposing the annealed ZrO_2(Si) film to UV irradiation, is photoquenched when subjected to 623 nm light. However, the *intensity* of the UV-induced EPR signal is *reduced* by approximately a factor of 10 (see Figs. 4 and 6) in the annealed films relative to this same feature in the as-deposited films.

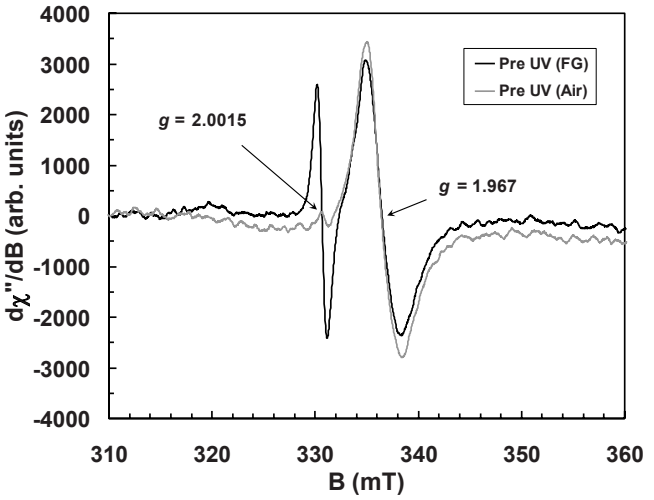

FIG. 5. EPR spectra at 77 K of ZrO_2(Si) film annealed in forming gas and in air at 350 °C for 10 h before exposure to UV (gain=6300).

C. ZrO_2(Si)/SiO_2 multilayer stack

Multilayer stacks consisting of alternating layers of ZrO_2(Si) and SiO_2 provide an opportunity to assess if the zirconia-silica *interfaces* contribute substantially to the occurrence of any specific defects. In Fig. 7, the spectra of an air-annealed (2.5 h at 460 °C) ZrO_2(Si)/SiO_2 multilayer stack are displayed. The $g=2.008$ feature following UV irradiation is clearly visible as well as the reduction in signal intensity following illumination with the photoquenching light at 623 nm. The other prominent spectral feature is at

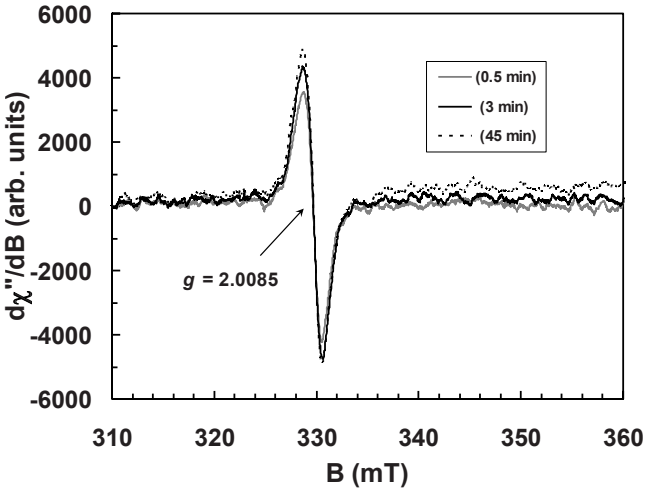

FIG. 6. EPR difference spectra of air-annealed ZrO_2(Si) film measured at 77 K. Sample first irradiated with UV then followed by illumination with 623 nm light for 0.5, 3, and 45 min (gain =4000). The spectra measured after 623 nm illumination were subtracted from the post-UV EPR spectrum.

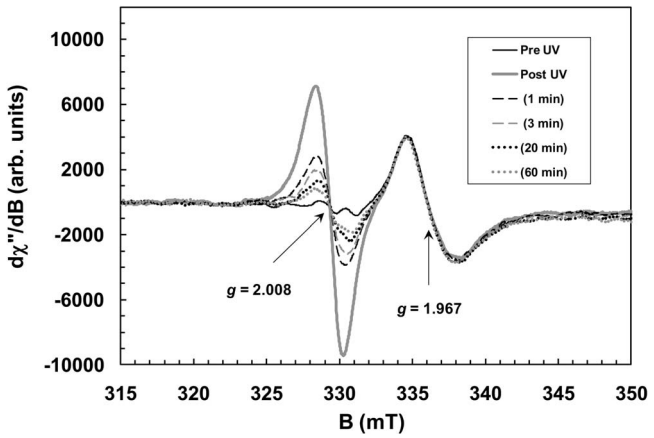

FIG. 7. EPR spectra of air-annealed multilayer stack measured at 77 K. Sample first irradiated with UV then followed by illumination with 623 nm light for 1, 3, 20, and 60 min.

$g=1.967$ and it is clear from the suite of EPR spectra that this resonance is not altered by either UV irradiation or the photoquenching light.

Shown in Fig. 8 are the difference spectra and as in the single layer ZrO_2(Si) films, the only spectral feature observed is the UV-induced resonance at $g=2.0085$. Based on the comparable signal strengths of the UV-induced center in the multilayer stack [$\sim 30 SiO_2/ZrO_2$(Si) interfaces] and the single thick ZrO_2(Si) film [one SiO_2/ZrO_2(Si) interface], we conclude that spectral contributions from defects located at interfacial sites are minimal and that the major contribution to the EPR intensity is due to UV-induced centers that are distributed uniformly throughout the thickness of the ZrO_2(Si) layers.

D. Isochronal anneal data

Isochronal anneal data were obtained for the as-deposited ZrO_2(Si) film discussed above. The sample was UV irradiated at 77 K and then transferred without warming to the Bruker variable-temperature dewar. The lowest temperature achieved in this nitrogen-flow dewar system was 94.2 K. Spectra were recorded as follows. The sample was rapidly warmed to a specific temperature and held there for 5 min, then cooled rapidly to 94.2 K and the spectrum recorded. No change in the EPR signal intensity of the UV-induced feature at $g=2.0085$ was observed until warming to ~ 180 K. Above this threshold temperature, the signal intensity of this feature decayed and a plot of the [EPR(T)/EPR(94.2 K)] versus T is shown in Fig. 9. It should also be pointed out that the signal intensity of the $g=1.967$ resonance was not thermally quenched when warmed to higher temperatures.

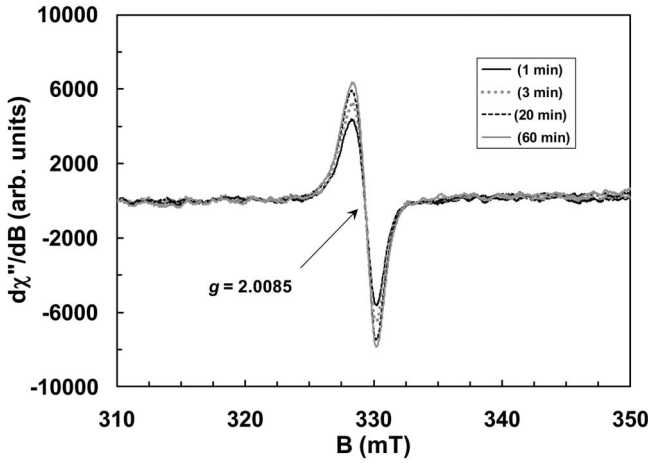

FIG. 8. EPR difference spectra of air-annealed multilayer stack measured at 77 K. Sample first irradiated with UV then followed by illumination with 623 nm light for 1, 3, 20, and 60 min. The spectra measured after 623 nm illumination were subtracted from the post-UV EPR spectrum.

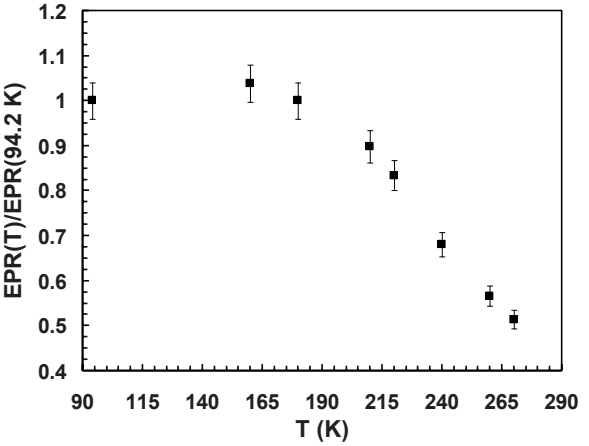

FIG. 9. Temperature dependence of the UV-induced EPR signal at $g=2.0085$ in as-deposited ZrO_2(Si) film.

IV. DISCUSSION

A. Si dependence of UV-induced center

In order to interpret the EPR data, it is important to have a structural model of the zirconia-silica solid solutions. It is also important to keep in mind that the spectra reported above were obtained from samples that contained $\sim 15\%$ SiO_2. As pointed out earlier, x-ray diffraction measurements revealed that all films were amorphous, with the exception of the nominally pure ZrO_2 film, which exhibited the peaks of monoclinic zirconia. This indicates the important role played by the incorporated Si in the solid solutions formed from ZrO_2 and SiO_2. Even at low levels, Si serves to stabilize the amorphous state. Several in-depth structural studies of $Zr_xSi_{(1-x)}O_2$, solid solutions over a broad compositional range (i.e., range for x) have been reported which indicate that the zirconia-silica alloy is amorphous provided annealing temperatures are kept well below 900 °C.[2,8,10–12] In particular, the experimental studies of Lucovsky and co-workers,[10,13] using a variety of techniques such as extended x-ray absorption fine-structure spectroscopy (EXAFS), x-ray photoelectron spectroscopy (XPS), Auger-electron spectroscopy (AES), and Fourier-transform infrared spectroscopy (FTIR), provided detailed information about the local bonding in pseudobinary zirconia silicates. This information was used to model the amorphous morphology

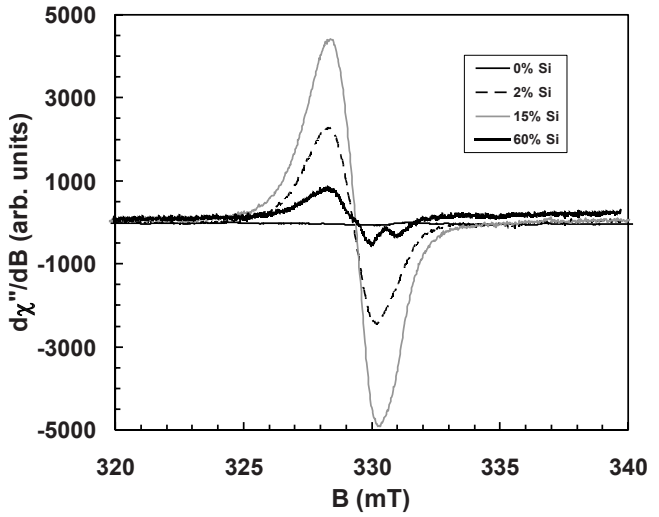

FIG. 10. Dependence of UV-induced EPR signal intensity at $g=2.0085$ on Si percentage of ZrO_2 layers in a multilayer stack.

and dielectric constants of a-$Zr_xSi_{(1-x)}O_2$ as a function of composition.[4,10,13]

We have observed that the EPR intensity of the UV-induced center is sensitive to the amount of Si incorporated in the $Zr_xSi_{(1-x)}O_2$ alloy. Shown in Fig. 10 is the dependence of the UV-induced EPR signal intensity at $g=2.0085$ on Si percentage of ZrO_2 layers. These data indicate the important role played by Si in creating/stabilizing potential pre-existing trapping sites capable of forming a UV-induced low-temperature stable paramagnetic center.

B. Model of UV-induced center

1. Local atomic configuration of $Zr_xSi_{(1-x)}O_2$ alloy

Detailed electronic structure calculations for zirconia silicate alloys are not currently available. Based on spectroscopic data presented in the literature[2,8,10] and molecular-dynamics simulations of *disordered zircon* ($ZrSiO_4$),[14] we will infer that the structure of the $Zr_xSi_{(1-x)}O_2$ solid solutions under investigation may be approximated as a *random close-packed* (rcp) structure, highly ionic in character.[15] In this model, which is strongly supported by the XPS and Auger electron spectroscopy,[10] atomic bonding considerations lead to local configurations such as Zr-O-Si, Zr-O-Zr, and Si-O-Si, having Zr-O and Si-O bond lengths similar or smaller[16,17] to those in crystalline zirconia[18] and fused silica,[19] respectively.

In amorphous materials, *color centers* arise from trapping free electrons or holes at pre-existing atomistic defects in the rcp structure, such as vacancies, over- or undercoordinated network atoms, interstitials, or impurities.[20] Even if the amorphous structure is perfectly bonded, i.e., the random close-packed structure is defect free (free from imperfections and extrinsic impurities), *self-carrier trapping* can still occur via *small polaron* formation or *Anderson localization*, which is a manifestation of the randomness of the network.[20,21] [We discuss below (Sec. IV D 1) recent theoretical electronic structure calculations devoted to the study of intrinsic bonding defects in crystalline HfO_2 and ZrO_2.] However, we note here that to date, the most comprehensively studied amorphous system is silica for the obvious reason that it is a key material used in silicon-based microelectronic devices and optical waveguide structures. In particular, the extensive studies by Griscom and co-workers,[22] devoted to understanding the electronic structure of point defects in amorphous silicon dioxide, provide some guidelines for modeling the atomistic nature of the UV-induced center observed in a-$Zr_xSi_{(1-x)}O_2$ solid solutions.

2. g-factor interpretation

The main spectroscopic feature is the measured g factor for the UV-induced center. No powder-averaged spectral features due to $\boldsymbol{g}$-tensor anisotropy were apparent; however, the line shape is not perfectly symmetrical and the line width is quite broad. The fact that the measured g factor is greater than the free-spin value indicates that the UV-induced center is a hole trap.[23] To investigate how the EPR line shape is modified by changes in the magnitude of $\boldsymbol{g}$-tensor anisotropy, powder EPR simulations were performed.[24] The computer simulations, using $\boldsymbol{g}$-tensor data reported in the literature for hole centers in a variety of materials,[23,25,26] suggest that resolving any anisotropic features would be difficult unless the variation of the principal components of the $\boldsymbol{g}$ tensor is in the range ± 0.008 assuming an intrinsic linewidth of ~ 1.6 mT.

Given that the UV-induced center is a hole-type center,[23,25,26] we suggest that a hole gets trapped on an oxygen atom associated with the local atomic grouping, Zr-O-Si. In the range of $x>0.5$, the a-$Zr_xSi_{(1-x)}O_2$ system can be visualized as an amorphous arrangement of Zr^{4+}, O^{2-}, and $[SiO_4]^{4-}$ ions. The hole is most likely trapped on an oxygen atom of the $[SiO_4]^{4-}$ ion, giving rise to a local atomic configuration $Zr^{4+}\cdots[\dot{O}\text{-}Si\equiv]^{3-}$, where $\equiv$ denotes the bonds to the three other oxygen atoms of the tetrahedrally shaped silicate ion. The hole may be self-trapped or stabilized by an *unidentified* defect, analogous to the oxygenic-hole centers observed in crystalline boron-doped $ZrSiO_4$.[25] Hole trapping at these sites is consistent with the observed dependence of the EPR intensity of the UV-induced center on Si density studied in this work.

It should be pointed out that ^{91}Zr, natural abundance of 11.2%, has a nuclear spin $I=5/2$ and should lead to detectable hyperfine features if unpaired electron-spin density resided on the ^{91}Zr atom in the Zr-O^--Si moiety.[26] However, no ^{91}Zr hyperfine features were observed in the measured spectra of the UV-induced center. This observation is not solely due to spectral resolution limitations associated with powder-averaged EPR spectra, but a consequence of the fact that the Zr-O bond is highly ionic and therefore, most of the spin densities reside on the Si-O^- portion of the trapped-hole complex.

3. Non-UV induced EPR centers

In the interest of being complete, we briefly discuss the EPR features observed prior to UV illumination. Shown in Fig. 1 is the EPR spectrum for the as-deposited film prior to UV irradiation. Clearly, when compared to Fig. 2, which

displays the EPR recorded on the same film after UV illumination, one notes that the EPR features in the unirradiated sample are significantly weaker. The resonance at $g=1.967$ has been reported extensively in the EPR literature on zirconia[27,28] and its interpretation as either Zr^{3+},[28] a paramagnetic oxygen vacancy,[29] or a Ti-related center[30] is still being debated. As pointed out above, the $g=1.967$ resonance intensity does not change when the film is subjected to UV illumination and its intensity in the as-deposited films is much weaker than the UV-induced resonance. These findings suggest that this line is not directly related to the formation and stability of the UV-induced center. Figure 5 displays spectra following annealing in forming gas and in air at 350 °C before exposure to UV illumination. It is interesting to note that annealing in either air or forming gas eliminates the $g>2.0023$ features; however, annealing in forming gas enhances the feature at $g=2.0015$. In addition, the $g=1.967$ resonance does not appear to be sensitive to the annealing atmospheres. Given that forming gas is a reducing atmosphere and that the strong resonance at $g=2.0015$ is less than the free-spin g value, it is reasonable to assign this feature to an electron-trap center. On the other hand, we are not able to make a positive assignment at this time of the spectral features in the $g \geq 2.002$ region in the as-deposited film prior to exposure to UV light (Fig. 1) since it is eliminated by annealing in air or forming gas. One can speculate that the thermal annealing process, regardless of environmental atmosphere, is sufficient to induce local structural changes that destabilize this trapping site. Finally, as discussed above, the assignment of the $g=1.967$ resonance to either Zr^{3+} or a paramagnetic oxygen vacancy is still in question; however, the fact that annealing in forming gas or air does not lead to a significant change in this feature provides supporting evidence for assigning the resonance to Zr^{3+}, which was most likely created during the deposition process.

C. Time dependence of the photoquenching measurements

We have also analyzed the photoquenching data of the UV-induced center as a function of 623 nm *illumination time* and the results are displayed in Fig. 11. The normalized amplitude of the EPR intensity of the UV-induced center was well fitted by the stretched-exponential function $N(t)=N_u+(1-N_u)\exp(-\Gamma_{str,1}t)^{\beta}$, where N_u represents the normalized amplitude at the quenching time $t=\infty$ (unquenchable centers), β is the stretch parameter which varies between 0 and 1, and $\Gamma_{str,1}$ is the stretched-exponential decay rate. The stretch parameter β characterizes the distribution of sites corresponding to different $\Gamma_{str,1}$'s in the amorphous film. It expresses the underlying distribution of rates: a small β implies a broad distribution of rates, whereas a β close to 1 is indicative of a narrow distribution.

In Fig. 11, the solid line was obtained using $N_u=0.26$, $\Gamma_{str,1}^{-1}=106\pm10$ s, and $\beta=0.47\pm0.05$. In the same figure displayed (dashed line) is the fit to the function $N(t)=N_o\exp(-\Gamma_{str,2}t)^{\beta}$, where N_o is the normalized amplitude at $t=0$, $\beta=0.26\pm0.05$, and $\Gamma_{str,2}^{-1}=494\pm50$ s. The latter function represents the case where all centers are photoquenchable and clearly does not appear to fit the data correctly.

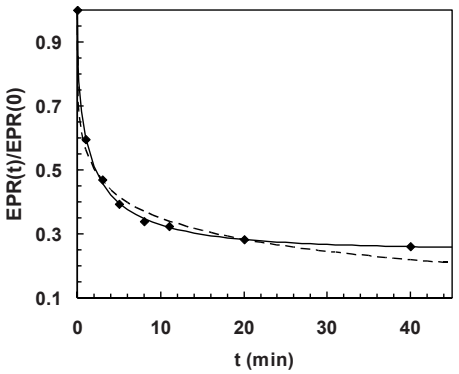

FIG. 11. UV-induced EPR intensity vs 623 nm photoquenching time. The solid diamonds are the experimental data points, the dashed line is a fit to $N(t)=N_o\exp(-\Gamma_{str,2}t)^{\beta}$, and the solid line through the data points is a fit to $N(t)=N_u+(1-N_u)\exp(-\Gamma_{str,1}t)^{\beta}$. See text for details.

The use of the stretched-exponential function to describe nonexponential decay in disordered systems has been around for many decades[31] and until only recently, it was regarded as a convenient functional form with limited physical significance. However, current research is focused on developing realistic microscopic models of relaxation in disordered systems in order to assign a physical basis to the stretch parameter β.[31,32] On the basis of our limited study, we suggest that the observed $\beta \approx 0.5$ may be indicative of dispersion in the carrier-trap distances, which is a consequence of the amorphous nature of the films.

D. Photophysical processes

1. Oxygen vacancies

In order to develop a basic understanding of the photophysical processes resulting in the creation and annihilation of the UV-induced center in a-$Zr_xSi_{(1-x)}O_2$ solid solutions, it is useful to examine recent electronic structure calculations on the related system, cubic ZrO_2.[33–35] One major point is that the valence-band edge consists mainly of O $2p$ states, whereas the conduction-band edge is mainly derived from Zr $4d$ states. The bonding, as indicated from the calculations, is typical of an ionic oxide consisting of Zr^{4+} and O^{2-} ions. These theoretical studies indicate that oxygen vacancies and oxygen interstitials are the dominating intrinsic bonding defects in bulk crystalline HfO_2 and ZrO_2. Specifically, the oxygen vacancy V_O^q can exist in five charge states $\{q=+2, +1, 0, -1, -2\}$, accommodating up to four electrons localized in the vicinity of the defect. The calculations locate, relative to the valence and conduction-band edges, the +1 and 0 charge states near midgap, whereas the −1 and −2 charged defect states are closer to the conduction-band edge.

Electrical measurements, combined with advanced spectroscopic techniques,[36,37] provide supporting evidence of the importance of these intrinsic defects in determining the properties of this class of high-κ gate dielectrics. In particular, Lucovsky and co-workers,[37,38] supported the view that *interstitial* O atom and O_2 molecule defect states are located in the lower half of the band gap within 1–2 eV of the valence-

band edge and may contribute to hole trapping. It should be pointed out, however, that the material systems studied by Lucovsky *et al.*[36–38] were 4–6-nm-thick films, annealed in inert nonoxidizing environments between 700 and 900 °C, which under these conditions lead to films with a nanocrystalline morphology. Furthermore, Lucovsky and co-workers[37,38] reported that their data provided experimental evidence for the clustering of defect states at nanocrystalline grain boundaries. For our amorphous films, this would correspond to an oxygen-excess defect in the local random close-packed environment.

2. Electron traps

As discussed above, we propose that the structure of the UV-induced center in a-$Zr_xSi_{(1-x)}O_2$ films is a trapped hole on the oxygen of a silicate group, i.e., $Zr^{4+}\cdots[\dot{O}\text{-}Si\equiv]^{3-}$. From recent electronic structure calculations on the related crystalline material $ZrSiO_4$,[39] we note that, as with crystalline ZrO_2, the O $2p$ states form the upper valence band while the Zr $4d$ states form the lower conduction band. The materials of interest in this study, however, are amorphous and it is well established that fluctuations in the short-range order lead to tailing of states into the band gap at the band edges. Because of band tailing, 253.7 nm (4.89 eV) photons have sufficient energy to generate electrons and holes via band-gap illumination; the holes in the valence band ultimately get localized on an oxygen atom associated with the silicate ion $[SiO_4]^{4-}$, while the electrons get trapped at the oxygen vacancies. Since we observe no *photoinduced* EPR resonance with a $g<2.0023$, indicative of an electron-trap center, there is no evidence for either V_O^- or V_O^+, thus we have to assume that the electrons exist in a spin-paired configuration, i.e., consistent with either V_O^0 or V_O^{2-} defect states.

3. Photoquenching mechanism

The photoquenching experiments reported here were carried out with 623 nm (1.99 eV) photons, which are not energetic enough to promote electrons from the valence band to the conduction band. We suggest, however, that the trapped hole is ionized to the valence band, i.e., $O^-+h\nu_{623\ \mathrm{nm}}\rightarrow O^{2-}+h^+_{\mathrm{VB}}$, and recombination between electrons (trapped at oxygen vacancies or other unspecified electron traps) and liberated holes leads to the photoquenching of the EPR signals associated with the UV-induced center. This is consistent with the use of a stretched-exponential function to describe the time-dependent photoquenching data discussed above, where the observed $\beta\approx 0.5$ is a signature of the dispersion in the carrier-trap distances.

Other channels for photoquenching the UV-induced center have been considered, such as optical excitation of the trapped hole followed by excitation-induced hopping to sites where electrons are trapped for recombination or electrons excited from traps followed by recombination with the trapped holes. At present, we reject these channels on the basis that we do not observe any new EPR signals at 77 K associated with electron excitation/trapping during the course of the photoquenching experiment. It should be pointed out that measurements at lower temperatures may prove useful for sorting out potential photoquenching mechanisms. However, it is possible that even at lower temperatures, the time scale for photoquenching dynamics may still be short compared to the time scale of the EPR measurement to yield spin-resonance signals that can be assigned to an electron excitation/trapping process.

As discussed above, given that the valence-band edge consists mainly of O $2p$ states and the amorphous nature of a-$Zr_xSi_{(1-x)}O_2$ solid solutions, hole localization should be facilitated by a suitable lattice distortion. Since the UV-induced center is stable only at low temperatures, we infer that the potential associated with the distortion is relatively shallow. The thermal quenching data presented in Fig. 9 show that this defect center is stable up to ~180 K, suggesting that above this temperature, holes localized by deformed surroundings are released due to thermal processes that relax the local deformation.

V. CONCLUSIONS

Amorphous thin films of $Zr_xSi_{(1-x)}O_2$, prepared on fused silica substrates, were investigated by EPR spectroscopy. A defect center was identified at $g=2.0085$ that is UV-light activated and photoquenched by red visible light. Its appearance is shown to depend on the amount of silicon in the films. We suggest that the UV-induced center in amorphous $Zr_xSi_{(1-x)}O_2$ films is a trapped *oxygenic-hole* center having the local atomic arrangement $Zr^{4+}\cdots[\dot{O}\text{-}Si\equiv]^{3-}$. Based on measurements at 77 K, we propose that photoquenching of the UV-induced centers with 623 nm photons is due to the photoionization of trapped holes to the valence band followed by recombination with trapped electrons. Photoquenching experiments are in progress at wavelengths greater than 623 nm and at lower temperatures in order to develop a better understanding of the recombination dynamics of the UV-induced oxygenic-hole center.

ACKNOWLEDGMENTS

We would like to thank Paul Adams for providing x-ray diffraction analysis, Nick Marquez for repeated SIMS analyses, and Sergio de la Torre for SEM/EDX analysis on some of our films. Chris Panetta grew some of the films investigated and Mark Ostrander cut and prepared all EPR samples. We would also like to thank Todd Rose for valuable suggestions after carefully reading the paper. This work was supported under The Aerospace Corporation's Independent Research and Development Program.

*heinrich.g.muller@aero.org

[1] B. A. van Hassel and A. J. Burggraaf, Appl. Phys. A: Mater. Sci. Process. **53**, 155 (1991).
[2] H. W. Chen, T. Y. Huang, D. Landheer, X. Wu, S. Moisa, G. I. Sproule, J. K. Kim, W. N. Lennard, and T. S. Chao, J. Electrochem Soc. **150**, C465 (2003).
[3] M. Houssa, A. Stresmans, M. Naili, and M. M. Heyns, Appl. Phys. Lett. **77**, 1381 (2000).
[4] G. Lucovsky, J. Vac. Sci. Technol. A **19**, 1553 (2001).
[5] D. A. Jaworske, NASA/TM Report No. 2000-210204, 2000 (unpublished).
[6] W. K. Kim, S. W. Kang, and S. W. Rhee, J. Vac. Sci. Technol. A **21**, L16 (2003).
[7] M. Lemberger, A. Pascaleva, S. Zürcher, A. J. Bauer, L. Frey, and H. Ryssel, J. Non-Cryst. Solids **322**, 147 (2003).
[8] G. Lucovsky, B. Rayner, Y. Zhang, G. Appel, and J. Whitten, Appl. Surf. Sci. **216**, 215 (2003).
[9] C. P. Poole, Jr., *Electron Spin Resonance*, 2nd ed. (Wiley-Interscience, New York, 1982).
[10] G. B. Rayner, Jr., D. Kang, Y. Zhang, and G. Lucovsky, J. Vac. Sci. Technol. B **20**, 1748 (2002).
[11] G. W. Wilk, R. M. Wallace, and J. M. Anthony, J. Appl. Phys. **87**, 484 (2000).
[12] G. B. Rayner, Jr., D. Kang, and G. Lucovsky, J. Vac. Sci. Technol. B **21**, 1783 (2003).
[13] G. Lucovsky and G. B. Rayner, Jr., Appl. Phys. Lett. **77**, 2912 (2000).
[14] R. Devanathan, L. R. Corrales, W. J. Weber, A. Chartier, and C. Meis, Phys. Rev. B **69**, 064115 (2004).
[15] R. Zallen, *The Physics of Amorphous Solids* (Wiley-Interscience, New York, 1983).
[16] V. Ramaswamy, B. Tripathi, D. Srinivas, A. V. Ramaswamy, R. Cattaneo, and R. Prins, J. Catal. **200**, 250 (2001).
[17] G. Mountjoy, R. Anderson, R. J. Newport, and M. E. Smith, J. Phys.: Condens. Matter **12**, 3505 (2000).
[18] D. K. Smith and H. W. Newkirk, Acta Crystallogr. **18**, 983 (1965).
[19] A. C. Wright, J. Non-Cryst. Solids **179**, 84 (1994).
[20] S. R. Elliot, *The Physics of Amorphous Materials* (Longman Inc., New York, 1983).
[21] N. F. Mott, Adv. Phys. **16**, 49 (1967).
[22] D. L. Griscom, J. Non-Cryst. Solids **352**, 2601 (2006), and references therein.
[23] B. Henderson and J. E. Wertz, Adv. Phys. **17**, 749 (1968).
[24] Bruker SIMFONIA software package.
[25] C. J. Walsby, N. S. Lees, W. C. Tennant, and R. F. C. Claridge, J. Phys.: Condens. Matter **12**, 1441 (2000).
[26] R. F. C. Claridge, K. M. Mackle, G. L. A. Sutton, and W. C. Tennant, J. Phys.: Condens. Matter **6**, 3429 (1994).
[27] C. Morterra, E. Giamello, L. Orio, and M. Volante, J. Phys. Chem. **94**, 3111 (1990).
[28] J. Matta, J.-F. Lamoinier, E. Abi-Aad, E. A. Zhilinskaya, and A. Aboukais, Phys. Chem. Chem. Phys. **1**, 4975 (1999).
[29] P. M. Lenahan and J. F. Conley, IEEE Trans. Device Mater. Reliab. **5**, 90 (2005).
[30] K. E. Swider and W. L. Worrell, J. Am. Ceram. Soc. **78**, 961 (1995).
[31] J. C. Phillips, Rep. Prog. Phys. **59**, 1133 (1996).
[32] L. Pavesi and M. Ceschini, Phys. Rev. B **48**, 17625 (1993).
[33] J. Robertson, K. Xiong, and B. Falabretti, IEEE Trans. Device Mater. Reliab. **5**, 84 (2005).
[34] J. Robertson, Rep. Prog. Phys. **69**, 327 (2006).
[35] J. L. Gavartin, D. M. Ramo, A. L. Shluger, G. Bersuker, and B. H. Lee, Appl. Phys. Lett. **89**, 082908 (2006).
[36] G. Lucovsky, D. M. Fleetwood, S. Lee, H. Seo, R. D. Schrimpf, J. A. Felix, J. Luning, L. B. Fleming, M. Ulrich, and D. E. Aspnes, IEEE Trans. Nucl. Sci. **53**, 3644 (2006).
[37] G. Lucovsky, H. Seo, S. Lee, L. B. Fleming, M. D. Ulrich, J. Luning, P. Lysaght, and G. Bersuker, Jpn. J. Appl. Phys. **46**, 1899 (2007).
[38] Y. M. Strzhemechny, M. Bataiev, S. P. Tumakha, S. H. Goss, C. L. Hinkle, C. C. Fulton, G. Lucovsky, and L. J. Brillson, J. Vac. Sci. Technol. B **26**, 232 (2008).
[39] R. Puthenkovilakam, E. A. Carter, and J. P. Chang, Phys. Rev. B **69**, 155329 (2004).